Rare Metal Materials and Engineering
Volume 55, Issue 8, August 2026
Available online at www.rmme.ac.cn

Science Press

Cite this article as: Li Zewen, Chen Hao, Chen Liyong, et al. Microstructure and Mechanical and Tribological Properties of WC-Co-Ce Cemented Carbide: First-Principles Calculations and Experiments[J]. Rare Metal Materials and Engineering, 2026, 55(08): 1876-1888. DOI: https://doi.org/10.12442/j.issn.1002-185X.20250550.

ARTICLE

Microstructure and Mechanical and Tribological Properties of WC-Co-Ce Cemented Carbide: First-Principles Calculations and Experiments

Li Zewen[1,2], Chen Hao[1,3], Chen Liyong[1,3,4], Zhang Jianbo[1], Zhang Fan[1], Xie Xiaolong[1,3]

[1] School of Materials Science and Engineering, Jiangxi University of Science and Technology, Ganzhou 341000, China; [2] School of Education, Nanchang Institute of Science and Technology, Nanchang 330108, China; [3] Engineering Research of Center of High-Efficiency Development and Application Technology of Tungsten Resources, Ministry of Education, Jiangxi University of Science and Technology, Ganzhou 341000, China; [4] Collaborative Innovation Center for Development and Utilization of Rare Metal Resources Co-sponsored by Ministry of Education and Jiangxi Province, Jiangxi University of Science and Technology, Ganzhou 341000 China

Abstract: The WC/Co and WC/CoCe interface models were constructed, and the interfacial energy, elastic constants, and charge distribution characteristics were calculated using first-principles calculations. WC-10Co, WC-10Co-0.5Ce, and WC-10Co-1Ce cemented carbides were fabricated via liquid-phase sintering. Microstructural analysis, mechanical testing, and friction and wear testing were conducted to investigate the influence of the rare earth element Ce on the overall performance of the cemented carbide. The calculated results indicate that doping with Ce promotes the formation of strong covalent bonds between W and Ce atoms at the interface, which increases the interfacial bonding energy, reduces the interfacial energy, and improves structural stability. Based on the elastic constants and electronic properties, it is predicted that the hardness, toughness, and wear resistance of the cemented carbide are enhanced. Experimental findings demonstrate that the optimal performance is achieved when the Ce content is 0.5wt%. At this concentration, the Vickers hardness reaches 1484 HV_{30}, the fracture toughness is 10.55 $MPa \cdot m^{1/2}$, and the wear rate is 1.067×10^{-5} $mm^3 \cdot N^{-1} \cdot m^{-1}$.

Key words: cemented carbide; first principles; interface model; mechanical properties; friction and wear

1 Introduction

WC-based cemented carbide is a high-performance material renowned for its exceptional hardness and wear resistance, which makes it widely applicable in fields such as mining, construction, cutting tools, wear-resistant components, aviation, and national defense[1–4]. The excellent wettability of Co on WC enables efficient densification during liquid-phase sintering, facilitating the production of high-performance composite materials. As a result, WC-Co cemented carbide remains the most prevalent type of cemented carbide used in industrial applications[5–7]. With the continuous expansion of application fields, the working conditions and performance requirements for cemented carbides are becoming increasingly demanding. Particularly under extreme working environments, where operational efficiency continues to rise, the service life of cemented carbide faces significant challenges[51]. Consequently, the development of high-performance cemented carbides with improved durability and extended service life is of considerable importance.

Rare earth elements, recognized as powerful additives in metallurgy, were introduced into cemented carbide by scholars as early as the 1960s. Over the subsequent decades, considerable progress has been made in this area. In recent years, investigations into the effects of rare earth elements on

Received date: October 27, 2025
Foundation item: Distinguished Professor Program of Jinggang Scholars in Institutions of Higher Learning; Jiangxi Province Double Thousand Plan Science and Technology Innovation High-End Talent Project (jxsq2019201039); Key Research and Development Project of Jiangxi Province (20224BBE51041); Supported by Collaborative Innovation Center for Development and Utilization of Rare Metal Resources Co-sponsored by Ministry of Education and Jiangxi Province (JXUST-XTCX-2024-03)
Corresponding author: Chen Hao, Ph. D., Professor, School of Materials Science and Engineering, Jiangxi University of Science and Technology, Ganzhou 341000, P. R. China, E-mail: chenhao@jxust.edu.cn

the properties of cemented carbides have attracted growing interest[8–10]. Li et al[11] prepared a novel rare-earth-modified cemented carbide with high hardness, high toughness, wear resistance, and corrosion resistance by incorporating CeO_2 via a two-step process, involving ball milling and spark plasma sintering. The results show that within the research scope, as the ball milling time increases, the grain size decreases. When the first step of ball milling reaches more than 48 h, the hardness of the obtained cemented carbide increases by 9.1%, and the fracture toughness increases by 25%. Yang et al[12] introduced rare earth oxides into WC-8Co cemented carbide via hot-press sintering and evaluated the performance based on density, hardness, and transverse rupture strength. They found that with the addition of 0.5wt% Y_2O_3/ZrO_2, the WC grain size reaches its minimum, accompanied by a 2.9% increase in hardness and a 46.6% improvement in flexural strength compared to those of undoped WC-8Co. Although numerous experimental studies have confirmed that rare earth doping can improve the performance of cemented carbides[13–16], understanding the underlying mechanisms, particularly from a microstructural perspective, presents challenges that are difficult to address through experimental methods alone. Therefore, the first-principles calculations have emerged as a powerful tool for elucidating the doping mechanisms of rare-earth elements[17–19]. The interface model is the most commonly used computational model in first-principles calculations for exploring the influence of atomic doping on the performance of polycrystalline materials. Currently, first-principles calculations have been successfully applied to various interface systems with different properties, including metal-to-metal and metal-to-ceramic interfaces[20–22]. Hao et al[23] constructed an interface model to examine the elastic constants, electronic properties, and thermodynamic behavior of Y-doped cemented carbide. Their results reveal the strengthened covalent bonding and increased interfacial bond energy in the Y-doped WC-Co system, along with increased shear and Young ' s moduli, suggesting concurrent enhancements in both hardness and toughness. Fan et al[24] used an interface model to calculate interfacial energy, work of adhesion, density of states (DOS), and charge density for La-doped cemented carbide. Results show a reduction in interfacial energy, an increase in adhesion work, and the enhanced covalent bonding across the interface, indicating greater interfacial stability. The rise in shear and Young ' s moduli further suggests the increase in interfacial bonding strength, overall toughness, impact resistance, and plasticity.

In recent years, advances in first-principles calculations have provided atomic-level insights into doping mechanisms. By constructing the WC/Co interface models and analyzing the interface energy, elastic constants, electronic properties, and diffusion kinetics, the effects of doped elements and material properties can be predicted, thereby guiding the design of experimental studies[25–30]. Previous research has primarily relied on experimental observations to assess the influence of rare earth elements on the properties of cemented carbides, supplemented by theoretical predictions of material performance. However, there have been relatively few studies about that theoretical calculations actively guided experimental work, or the accuracy of computational predictions was systematically validated through experimental results. This study focused on rare-earth Ce-doped WC-Co cemented carbide. Through the combination of first-principles calculations and experimental research, this study aimed to reveal the influence of the element Ce on the interface structure, electronic properties, and mechanical and tribological properties of WC-Co, and to develop a new type of cemented carbide with high hardness, high toughness, and strong wear resistance.

2 Interface Model and Calculation Method

All density functional theory calculations in this study were conducted using the Vienna AB-initio Simulation Package, adopting the generalized gradient approximation of Perdew-Burke-Ernzerhof (GGA-PBE) function. The energy convergence threshold was 1×10^{-5} eV, and the force convergence criterion was −0.01 eV. The cutoff energy of the plane wave was 520 eV. The K-point grid was set to 7×7×1. In previous studies, Co, as a binder, exhibited excellent wettable properties on the surface of WC particles during the liquid-phase sintering process, and the molten Co filled the gaps between WC particles through capillary action[31]. According to previous studies, the $WC_{(0001)}$ is the lowest-energy and most stable surface in the WC structure and is usually used as the base surface for interface calculations[5,23]. Through calculation, the $Co_{(111)}$ surface has the lowest energy and the best lattice match with the $WC_{(0001)}$ surface in the crystal structure. Experimental studies using an atomic probe tomograph[32–33] have shown that almost all detected WC/WC grain boundaries contain separated thin Co layers. Accordingly, a three-layer Co model was selected to represent this thin layer. Studies have shown that in the microstructure of rare earth cemented carbides, there are no rare earth elements in the WC phase, but there are rare earth elements in the grain boundaries and the adhesive Co phase[12]. Therefore, the structure model of rare-earth cemented carbide can be regarded as one in which rare-earth elements replace part of the Co atoms in the model. The crystal structures of WC and Co are shown in Fig. 1. In this study, the energies of four distinct doping sites at the interface were computed to identify the most stable Ce doping configuration, corresponding to the lowest energy structure, as illustrated in Fig.2. Based on these

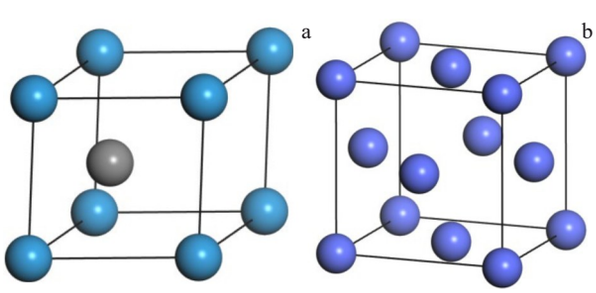

Fig.1 Schematic diagrams of crystal structures of WC (a) and Co (b)

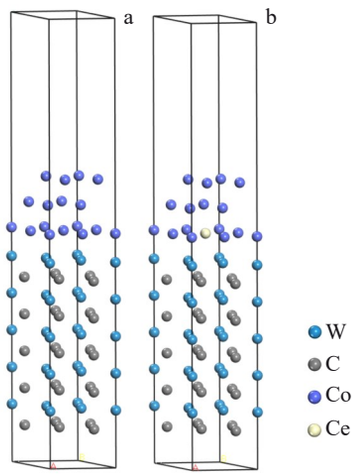

Fig.2 Schematic diagrams of interface models of WC/Co (a) and WC/CoCe (b)

results, the WC/Co and WC/CoCe interface models in Fig. 2 were established.

3 Experiment

Ball milling was conducted using Co powder (provided by Hebei Hangbai Metal Materials Co., Ltd, purity>99.9%, 3.0–5.0 μm, 10wt%), rare earth powder (provided by Aladdin Company, purity>99.99%, 1.0–3.0 μm, 0.5wt% or 1wt% of element Ce), WC powder (provided by Hebei Hangbai Metal Materials Co., Ltd, purity>99.99%, 1.0–3.0 μm, surplus), and liquid paraffin of 2.0% as raw materials. The scanning electron microscope (SEM) images of the three powders are shown in Fig. 3. Ball milling was performed using jars made of hard alloy and hard alloy balls with diameters of 6, 8, and 10 mm, which can prevent the introduction of other impurities during the ball milling process and avoid the contamination of raw materials. Anhydrous ethanol was used as the ball milling solvent. The ratio of balls to materials was set at 8∶1, the ball milling speed was 220 r/min, and the ball milling time was uniformly set at 12 h. Finally, the mixed powder was placed in a vacuum drying oven with the drying temperature at 80 ℃ for 5 h. The dried powder was sieved through the 180 μm sieve to obtain WC-Co-Ce composite powder[34–35].

The composite powder of 15 g was poured into a hard alloy mold with a diameter of 20 mm. After holding at 300 MPa by a hydraulic press (Model TH106-30T) for 20 s, the composite was placed in an atmosphere sintering furnace (Model GSL-1600X) for sintering. The schematic diagram of sintering process is shown in Fig. 4. After obtaining the cemented carbide, the sintered cemented carbides were characterized by SEM (MLA-650) coupled with an energy-dispersive X-ray spectroscope (EDS). X-ray diffractometer (XRD) was also used. Vickers hardness (load of 30 kg), fracture toughness (indentation method with load of 30 kg), and friction and wear performance (reciprocating friction and wear test for 1 h) were measured.

The microstructure, friction and wear morphology, and elemental distribution of the samples were identified by SEM and EDS. The density of the sample was determined using an AU-600ME alloy densitometer. The hardness and fracture toughness of the samples were tested using the

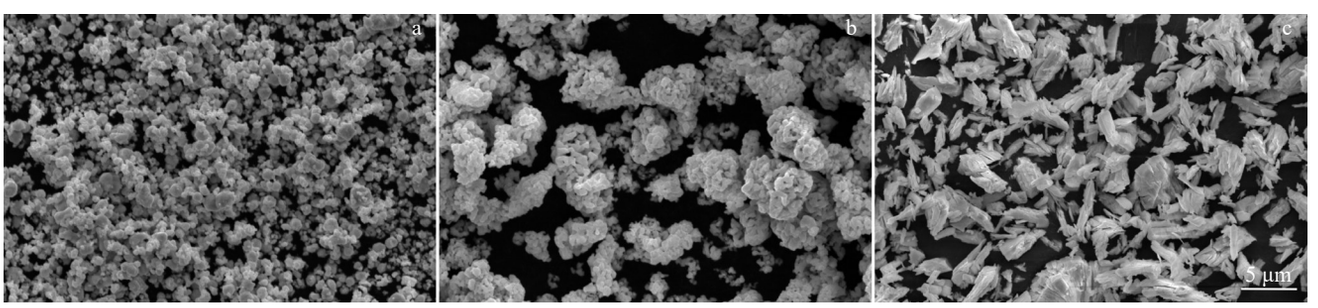

Fig.3 SEM images of raw powders: (a) WC; (b) Co; (c) Ce

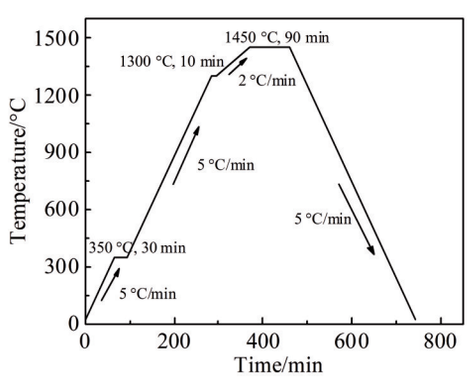

Fig.4 Schematic diagram of sintering process

FUTURE TECH fully automatic micro-Vickers hardness measurement system. The wear test was conducted on the HRS-2 M reciprocating sliding wear testing machine (load of 80 N; rotational speed of 300 r/min). The three-dimensional morphology of the wear marks was characterized by the NanoMap 500 LS three-dimensional surface topography instrument, while the two-dimensional morphology was characterized by the MT-500 wear testing machine.

4 Results and Discussion

4.1 Interface performance

In crystallography, when two crystals or their combination exist, there is a boundary, which is the interface. The stability

of the interface is a necessary condition for the formation of new structures. Surface energy can be used to measure the stability of the interface[36]. The formula for surface energy (E_{surf}) is as follows:

$$E_{surf}=\frac{E_{slab}-\left(\frac{N_{slab}}{N_{bulk}}\right)E_{bulk}}{2A} \tag{1}$$

where E_{slab} represents the energy of the optimized unit cell surface; E_{bulk} represents the total energy of the optimized unit cell; N_{slab} represents the number of atoms on the crystal plane; N_{bulk} represents the total number of atoms in the unit cell; A represents the interface area.

Adhesion work is a quantitative description of the minimum work required by the external force when two connected substances separate from the interface. It directly reflects the strength of the interface bonding between the two substances. The greater the adhesion work, the stronger the interfacial bonding (W_{ab}) [37]. It can be calculated by the following formula:

$$W_{ab}=\frac{E_a+E_b-E_{ab}}{S} \tag{2}$$

where E_{ab} is the total energy of the interface formed by surfaces A and B; E_a is the total energy of the A side; E_b is the total energy of the B side; S represents the interface area.

If surface A combines with surface B to form an interface, the interface atoms will rearrange, causing a change in the system energy. This stored additional energy is the interface energy (γ) [38], which can be calculated by the following formula:

$$\gamma=\sigma_1+\sigma_2-W_{ab} \tag{3}$$

where σ_1 and σ_2 are the surface energies of surface A and surface B, respectively.

The calculated values of interface energy of WC/Co and WC/CoCe cemented carbides are shown in Table 1. A low interfacial energy $E_{interface}$ indicates that the atoms of the two phases interact strongly at the interface, and that greater energy is required during separation, making them difficult to separate. A high interfacial energy, on the other hand, reflects weak atomic bonding at the interface, making the separation easier. It can be known from Table 1 that the WC/CoCe interface energy is lower, and the interface bonding is more stable.

4.2 Elastic constant

Elastic constants provide a quantitative description of the mechanical behavior of materials based on the atomic scale. By applying a small strain to the material and calculating its stress response, the elastic constant C_{ij} can be used to analyze the stiffness, anisotropic characteristics, mechanical stability, and resistance to deformation of the material, thereby laying a solid theoretical foundation for predicting the macroscopic mechanical properties of the material, including hardness, strength, and fracture toughness[39–40].

The interface structures of WC/Co and WC/CoCe both belong to the monoclinic crystal system. The mechanical stability standard that meets the monoclinic crystal system is as follows[23,41]:

$$C_{ii}>0,\ \mathrm{i}=1\text{–}6 \tag{4}$$

$$C_{11}+C_{22}+C_{33}+2(C_{12}+C_{13}+C_{23})>0 \tag{5}$$

$$C_{33}C_{55}-C_{35}^2>0,\ C_{44}C_{66}-C_{46}^2>0,\ C_{22}+C_{33}-2C_{23}>0 \tag{6}$$

$$[C_{22}(C_{33}C_{55}-C_{35}^2)+2C_{23}C_{25}C_{35}-C_{23}^2C_{55}-C_{25}^2C_{33}]>0 \tag{7}$$

$$\begin{aligned}&\{2[C_{15}C_{25}(C_{33}C_{12}-C_{13}C_{23})+C_{15}C_{35}(C_{22}C_{13}-C_{12}C_{23})\\&+C_{25}C_{35}(C_{11}C_{23}-C_{12}C_{13})]-[C_{15}^2(C_{22}C_{33}-C_{23}^2)\\&+C_{25}^2(C_{11}C_{33}-C_{13}^2)+C_{35}^2(C_{11}C_{22}-C_{12}^2)]+C_{55}\Delta\}>0\end{aligned} \tag{8}$$

$$\begin{aligned}\Delta=&C_{13}(C_{12}C_{23}-C_{13}C_{22})+C_{23}(C_{12}C_{13}-C_{23}C_{11})\\&+C_{33}(C_{11}C_{22}-C_{12}^2)\end{aligned} \tag{9}$$

Both the WC/Co and WC/CoCe structures meet the above conditions, indicating that the two structures are stable. The mechanical properties of cemented carbide, such as toughness, stability, and hardness, are closely related to the elastic constant. Therefore, the elastic constants of the two materials were calculated, as shown in Table 2.

For the monoclinic crystal system, the product moduli (B_V and B_R) and shear moduli (G_V and G_R) of the Voigt and Reuss polycrystals are as follows:

$$G_V=1/15[C_{11}+C_{22}+C_{33}+3(C_{44}+C_{55}+C_{66})-(C_{12}+C_{13}+C_{23})] \tag{10}$$

$$\begin{aligned}G_R=&15\{4[C_{11}(C_{22}+C_{33}+C_{23})+C_{22}(C_{33}+C_{13})\\&+C_{33}C_{22}-C_{12}(C_{23}+C_{12})-C_{13}(C_{12}+C_{13})\\&-C_{23}(C_{13}+C_{23})]/\Delta+3\left(\frac{1}{C_{44}}+\frac{1}{C_{55}}\frac{1}{C_{66}}\right)\}^{-1}\end{aligned} \tag{11}$$

$$B_V=1/9[C_{11}+C_{22}+C_{33}+2(C_{12}+C_{13}+C_{23})] \tag{12}$$

$$\begin{aligned}B_R=&\Delta[C_{11}(C_{22}+C_{33}-2C_{23})+C_{22}(C_{33}-2C_{13})\\&-2C_{33}C_{12}+C_{12}(2C_{23}-C_{12})+C_{13}(2C_{12}-C_{13})\\&+C_{23}(2C_{13}-C_{23})]^{-1}\end{aligned} \tag{13}$$

The mechanical properties were further calculated. The volume modulus B_H, shear modulus G_H, Young's modulus E,

Table 1 Calculated values of interface energy of WC/Co and WC/CoCe cemented carbides

Parameter	$E_{interface}$/eV	E_{WC}/eV	E_{binder}/eV	A/×10^{-2} nm^{-2}	W_{ab}/J·m^{-2}	γ/J·m^{-2}
WC/Co	–407.432	–324.713	–78.238	22.164	3.238	3.807
WC/CoCe	–408.792	–324.713	–79.309	22.185	3.445	3.176

Note: E_{WC} represents the energy of WC surface, and E_{binder} refers to the energy of the other phase interface.

Table 2 Calculated elastic constants of WC/Co and WC/CoCe cemented carbides

Elastic contant	C_{11}	C_{22}	C_{33}	C_{44}	C_{55}	C_{66}	C_{12}	C_{13}	C_{15}	C_{23}	C_{35}	C_{46}
WC/Co	335.8	442.3	415.5	171.9	39.0	53.3	93.1	38.5	0.0	48.2	0.0	0.0
WC/CoCe	395.6	453.1	413.9	170.6	39.2	62.2	85.8	73.6	0.0	48.1	0.0	0.0

and Poisson's ratio σ were calculated using the Voigt-Reuss-Hill (VRH) approximation method. The formulas are as follows:

$$G_H = \frac{1}{2}(G_V + G_R) \quad (14)$$

$$B_H = \frac{1}{2}(B_V + B_R) \quad (15)$$

$$E = \frac{9B_H G_H}{3B_H + G_H} \quad (16)$$

$$\sigma = \frac{3B_H - 2G_H}{2(3B_H + G_H)} \quad (17)$$

Based on the VRH approximation, the results of the volumetric modulus B_H, shear modulus G_H, the ratio of volumetric modulus to shear modulus B_H/G_H, Young's modulus E, and Poisson's ratio σ are shown in Table 3. It can be known from Table 3 that both the shear modulus and the volumetric modulus of WC/CoCe are slightly greater than those of WC/Co. The volumetric modulus reflects the resistance to volume change. The compressibility of WC/CoCe is higher than that of WC/Co. The shear modulus is related to hardness. The higher the shear modulus of a material, the higher the hardness, indicating that the hardness of WC/CoCe is higher. Young's modulus indicates the stiffness and hardness of materials. The greater the Young's modulus of a material, the greater the hardness and stiffness. It can be known that WC/CoCe has greater stiffness and higher hardness.

The ratio of bulk modulus to shear modulus (B_H/G_H), proposed by Pugh, can be used to evaluate the toughness and brittleness of materials. The higher the B_H/G_H ratio, the greater the toughness of the material, while a lower B_H/G_H value indicates brittleness. The critical value standard for generally evaluating toughness and brittleness is approximately 1.75. When B_H/G_H<1.75, the material is brittle; conversely, it is ductile[42].

As shown in Table 3, WC/Co exhibits slightly brittle properties, while WC/CoCe cemented carbide shows toughness. In addition, Poisson's ratio σ can also reflect the brittleness and toughness of materials, and its value range is usually from –1 to 0.5. The larger the Poisson's ratio, the better the toughness of the material. If it is higher than 0.26, the material has better ductility. The Poisson's ratio of WC/CoCe cemented carbide is larger, and it has better ductility.

Table 3 Parameter values of elastic property of WC/Co and WC/CoCe cemented carbides

Parameter	G_H/GPa	B_H/GPa	B_H/G_H	E/GPa	σ
WC/Co	100.159	171.288	1.710	251.463	0.255
WC/CoCe	104.825	184.190	1.757	264.492	0.273

4.3 Electronic characteristics

DOS and partial density of states (PDOS) are important tools for analyzing electronic structures. They reflect the distribution of electron energy in the Brillouin zone along high-symmetry directions (i. e., their dependence on the ***k*** vector) and qualitatively depict the electronic characteristics of materials. To compare the bonding strength and performance of the WC/Co and WC/CoCe interfaces, the total density of states (TDOS) and PDOS in the equilibrium geometric configuration (within the GGA-PBE framework) were calculated and analyzed. These results are helpful for understanding the combined characteristics of the interface.

As shown in Fig. 5, TDOS of WC/Co and WC/CoCe exhibits similar shapes. This suggests similar bulk moduli for the two interfaces. The electronic states in the energy range from –10 eV to –5 eV are primarily contributed by the C-s and W-d orbitals. The energy of WC/Co within the range from –5 eV to 5 eV is mainly contributed by the W-d, C-p, and Co-d orbitals, and that of WC/CoCe is mainly contributed by the W-d, C-p, Co-d, and Ce-d orbitals. For WC/Co, the energy range of 5–10 eV, is mainly contributed by the W-d orbital, while for WC/CoCe, it is mainly contributed by the W-d and Ce-d orbitals.

Furthermore, WC/Co and WC/CoCe have no band gap at the Fermi level, and the DOS value at the Fermi level is significantly greater than 0, indicating that both WC/Co and WC/CoCe exhibit metallic properties[21,25]. The DOS value of WC/CoCe at the Fermi level is less than that of WC/Co, and the DOS value of WC/Co at the Fermi level is 30.15. The DOS value of WC/CoCe is 24.03. WC/Co exhibits a broad and relatively flat peak near the Fermi level, which is indicative of high electronic conductivity[43], while WC/CoCe exhibits a sharper localized peak. This is because the 4f

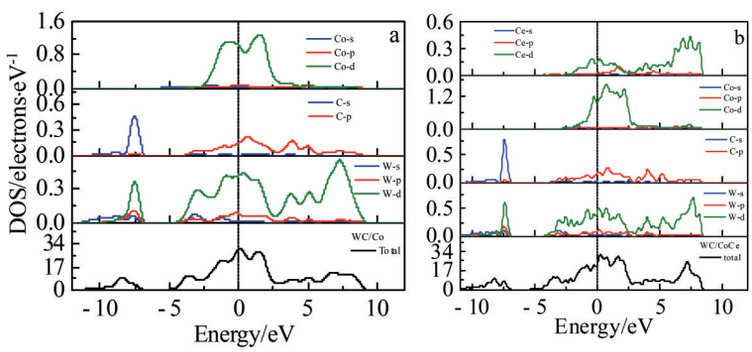

Fig.5 DOS of WC/Co (a) and WC/CoCe (b) cemented carbides

electron orbital of Ce enhances the electron correlation, and the local state scattering conducts electrons, reducing the metallic properties of the cemented carbide[44]. It is also observed that Ce-P and W-d have obvious resonance phenomena. It indicates that Ce and W atoms hybridize to form additional covalent bonds. Compared with the W-Co bond of WC/Co, Ce-W hybridization enhances the covalent bond composition. The stronger Ce-W covalent bonding contributes to the higher hardness predicted for WC/CoCe, which is consistent with the experimentally observed improvement in wear resistance upon Ce addition.

Fig.6 shows the electron localization function (ELF) results of WC/Co and WC/CoCe. Fig.6a is ELF of WC/Co. The WC region shows a high degree of localization, which is a typical feature of carbides——the strong covalent bond characteristic of the W-C bond. The interface region shows a moderate localization, indicating that there is a metal-covalent mixed bond in the W-Co bond. The upper part of the Co region shows typical characteristics of metal-bond delocalization. Fig. 6b shows ELF of WC/CoCe. Firstly, it is observed that there is a highly localized phenomenon around the Ce atoms. This is due to the strong localization effect of the 4f electrons of Ce. Ce attracts surrounding electrons, resulting in an increase in interface charge density. It can be further observed that the electronic localization at the interface is enhanced and the electron cloud is broken, while the electron cloud at the WC/Co interface is continuous. This indicates that at the WC/CoCe interface, covalent bonds are mainly dominant, followed by metallic bonds, while at the WC/Co interface, metallic bonds are dominant, followed by covalent bonds. Therefore, the addition of Ce is beneficial to improving the interfacial bonding strength and hardness of cemented carbide.

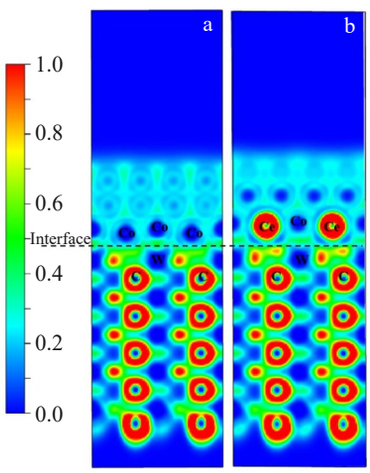

Fig.6 ELF results of WC/Co (a) and WC/CoCe (b) cemented carbides

4.4 Microstructure

Fig.7 shows the microstructures and XRD patterns of three types of WC-based cemented carbides with different Ce contents. Fig. 7a shows the microstructure of WC-10Co cemented carbide. The grain size of WC is the largest, and Co acts as a binder to wrap around WC. The grains present polygonal and triangular morphologies. After adding 0.5wt% Ce, the grain size of WC decreases, and the grains present a relatively uniform plate-like morphology. At the Ce content of 1wt% , the grain distribution remains relatively uniform; however, some plate-like grains exhibit coarsening phenomena. These phenomena indicate that the addition of element Ce can effectively inhibit the growth of grains and promote the uniform distribution of the microstructure. Fig.7d shows XRD patterns of WC-based cemented carbides with different Ce contents. It is observed that the peaks of all

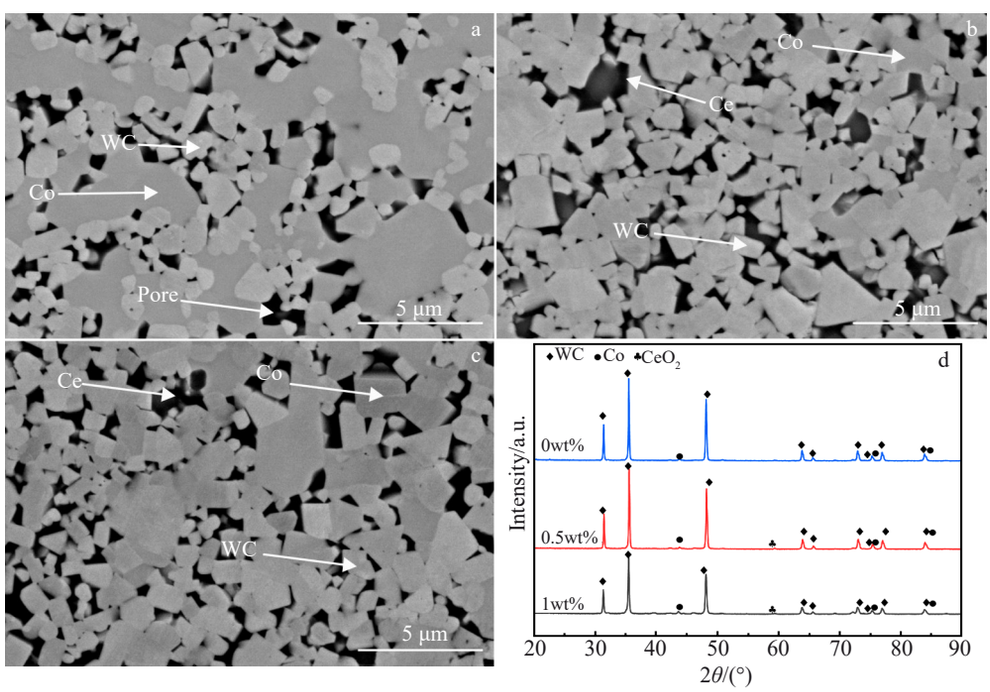

Fig.7 Microstructures (a–c) and XRD patterns (d) of WC-10Co cemented carbides with different Ce contents: (a) 0wt%; (b) 0.5wt%; (c) 1wt%

cemented carbides are approximately the same, with three sharp WC phase peaks and several weak ones. The Co phase has a weak peak near 44°. Furthermore, there are weak peaks near 59° in XRD pattern with the addition of the element Ce, corresponding to the peaks of the CeO_2 phase. Their peak heights are not obvious because the added amount is really too small.

Fig. 8 presents SEM images and corresponding EDS element mappings of WC-10Co cemented carbides with different Ce contents. Upon the addition of 0.5wt% Ce, the element Co exhibits a more uniform distribution throughout the cemented carbide matrix, while the element Ce is also homogeneously dispersed and partially precipitated to form a Ce-rich phase. Upon the addition of 1wt% Ce, the Co phase remains uniformly distributed, and Ce begins to show a slight tendency toward local aggregation. With the further increase in Ce content, a pronounced agglomeration of Ce is observed. This suggests that excessive Ce addition does not contribute to further grain refinement.

4.5 Mechanical properties

Fig. 9 shows the density and relative density of WC-10Co cemented carbides with different Ce contents. It can be seen that both the density and relative density of the cemented carbide increase after Ce doping. Among them, the relative density of the cemented carbide doped with 0.5wt% Ce is the highest, reaching 98.45%. The relative density of WC-10Co cemented carbide is only 96.69%. This is primarily because the addition of the element Ce can effectively inhibit the abnormal growth of WC grains and prevent the formation of closed macropores that are difficult to eliminate. However, at the Ce content of 1wt%, Ce begins to agglomerate. When these aggregates increase, they become defects and thereby hinder densification.

Fig. 10 shows the hardness indentation and crack morphologies, as well as the Vickers hardness and fracture toughness results of cemented carbides with different Ce contents. Fracture toughness (K_{IC}) is calculated based on Vickers hardness and the total crack length[45]. The calculation formula is as follows:

$$K_{IC} = 0.15\sqrt{\frac{HV_{30}}{\Sigma L}} \quad (18)$$

where HV_{30} is the Vickers hardness obtained under a load of 294 N, and ΣL is the total length of the crack.

The Vickers hardness of the WC-10Co cemented carbide is 1376 HV_{30}, and the fracture toughness is 8.71 MPa·$m^{1/2}$. After adding the element Ce, both the Vickers hardness and toughness of the cemented carbide are improved. When the addition amount is 0.5wt%, the Vickers hardness is 1484 HV_{30},

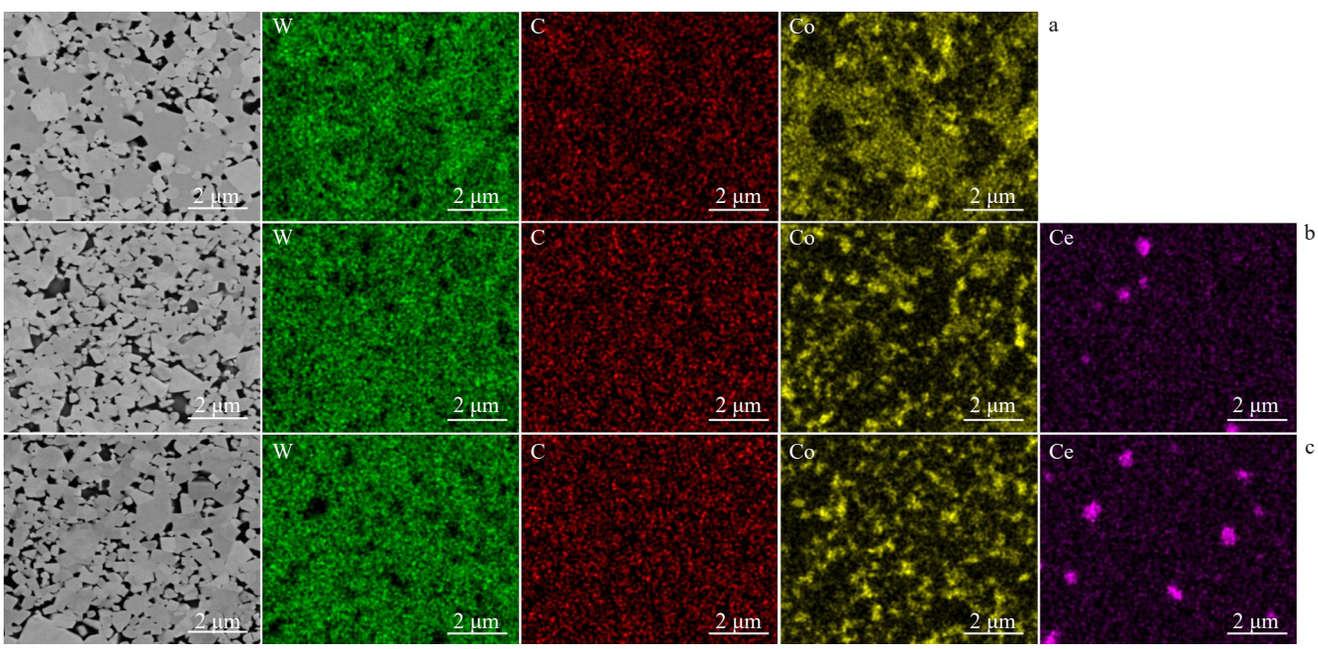

Fig. 8 SEM images and corresponding EDS element mappings of WC-10Co cemented carbides with different Ce contents: (a) 0wt%; (b) 0.5wt%; (c) 1wt%

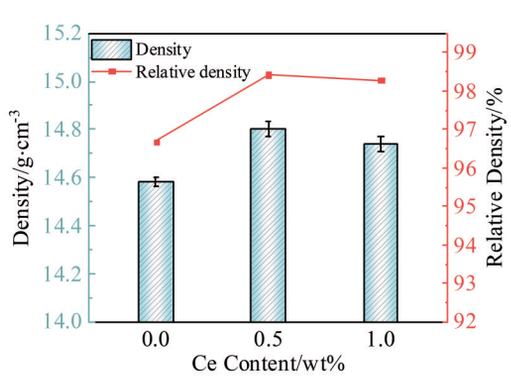

Fig. 9 Density and relative density of WC-10Co cemented carbides with different Ce contents

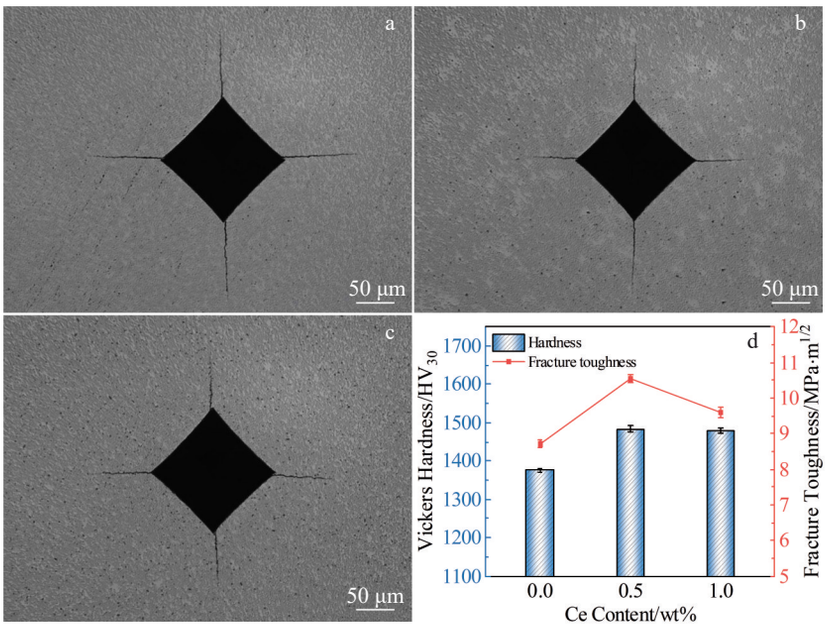

Fig.10 Crack morphologies (a–c) and Vickers hardness and fracture toughness results (d) of WC-10Co cemented carbides with different Ce contents: (a) 0wt%; (b) 0.5wt%; (c) 1wt%

and the fracture toughness reaches 10.55 MPa·m$^{1/2}$. Based on first-principles calculations, it is known that the incorporation of element Ce enhances the interfacial bonding strength of WC/Co. The 4f electrons of Ce have high localization and activity, forming strong covalent-ionic mixed bonds with surrounding atoms, which makes the interfacial bonding strength of the cemented carbide higher. Stronger interfacial bonding means that during the indentation process, it is more difficult for external forces to dissipate energy through interfacial sliding or debonding. The ability of the material to resist plastic deformation (i.e., hardness) is enhanced. Cracks are also more difficult to propagate along the weakened interface. Stronger interfacial bonding can effectively prevent cracks from preferentially spreading along the interface in the intergranular fracture mode at the WC/Co interface (intergranular fracture is brittle). It forces the crack to fracture more intergranular or transfer the load more effectively from the fractured WC grains to the adjacent Co phase and the unfractured WC grains, requiring more energy to propagate the crack, thereby enhancing the fracture toughness. A stronger interface also means that the Co phase can bridge cracks more effectively, undergo plastic deformation, and absorb energy.

4.6 Friction and wear performance

The evolution of the coefficient of friction (COF) with time during reciprocating sliding tests is shown in Fig. 11a. The variation patterns of all COF curves are approximately the same. During the first 5 min of the reciprocating friction process, due to the running-in period, the COF value gradually increases. With the friction proceeding, all COF curves tend to stabilize, indicating that the friction process enters the stable period[46–49]. The COF of the cemented carbide with 0.5wt% Ce is the lowest, followed by that with 1wt% Ce. The COF of pure WC-10Co cemented carbide is the highest. The average COF values, calculated from the steady-state period (after the initial 5 min), are presented in Fig. 11b. The cemented carbide with 0.5wt% Ce exhibits the lowest average COF of 0.397. The average COF of cemented carbide without the element Ce is 0.490. This improvement can be attributed to the enhanced interfacial bonding strength and increased

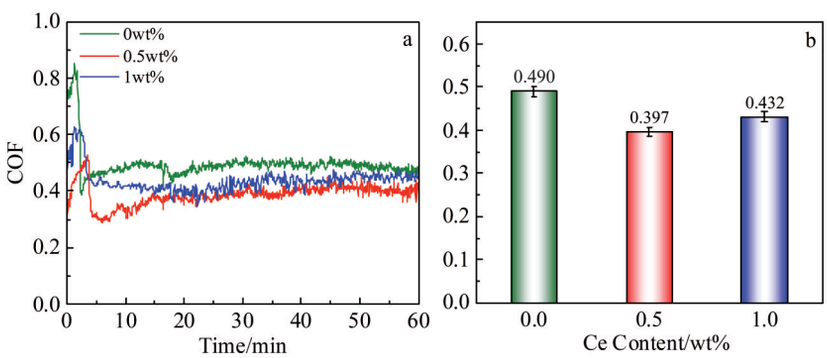

Fig.11 COF curves (a) and average COF (b) of WC-10Co cemented carbides with different Ce contents

bond energy induced by Ce addition, leading to improved hardness and toughness. These properties reduce the tendency for abrasive debris formation and improve wear resistance under applied stress. However, when the content of element Ce reaches 1 wt%, element Ce begins to aggregate, forming brittle phases and inclusions, and the wear resistance decreases instead.

Fig.12 shows the 2D and 3D profiles of the wear scars after the reciprocating friction test. After measurement, the relevant parameters of the sample wear scars are presented in Table 4, and Fig. 13 shows the wear rates of the three cemented carbides obtained through calculation. The wear rate of WC-10Co cemented carbide is approximately 1.213×10^{-5} $mm^3\cdot N^{-1}\cdot m^{-1}$. After adding 0.5wt% Ce, the wear rate decreases to 1.067×10^{-5} $mm^3\cdot N^{-1}\cdot m^{-1}$. When the doping amount of Ce is 1wt%, the wear rate of the cemented carbide increases to 1.150×10^{-5} $mm^3\cdot N^{-1}\cdot m^{-1}$. The cemented carbide doped with 0.5wt% Ce exhibits the lowest wear volume, whose width, depth, cross sectional area, and wear volume of the wear scars all reach the minimum values, which are 1.351 mm, 37.386 μm, 0.0308 mm^2, and 0.1536 mm^3, respectively. At this time, the wear resistance of the cemented carbide is the best. However, when the Ce content reaches 1wt%, the wear resistance is not as good as at 0.5wt%, but it is better than that of pure WC-10Co cemented carbide. The cause of this phenomenon is consistent with the results of the previous calculation. The appropriate addition of Ce strengthens the interface bonding, increases the bonding energy, and increases both the Young's modulus and Poisson's ratio of the cemented carbide, which further improves the hardness of the cemented carbide. The ratio of the volume modulus to the shear modulus of the Ce-doped cemented carbide exceeds the critical value of 1.75. The Ce-doped cemented carbide shows improved toughness. Meanwhile, the addition of Ce produces a fine-grained strengthening effect, which can inhibit abnormal grain growth and improve the wear resistance of the cemented carbide. With the increase in Ce content, the wear resistance of the cemented carbide decreases instead, indicating that the appropriate addition amount of Ce is very important for improving the wear resistance of the cemented carbide.

Fig. 14 shows the morphologies of the wear scars of WC-10Co cemented carbides with different Ce contents after the reciprocating friction and wear test. Under identical stress and duration conditions, the cemented carbide without Ce exhibits severe wear, characterized by extensive scratching.

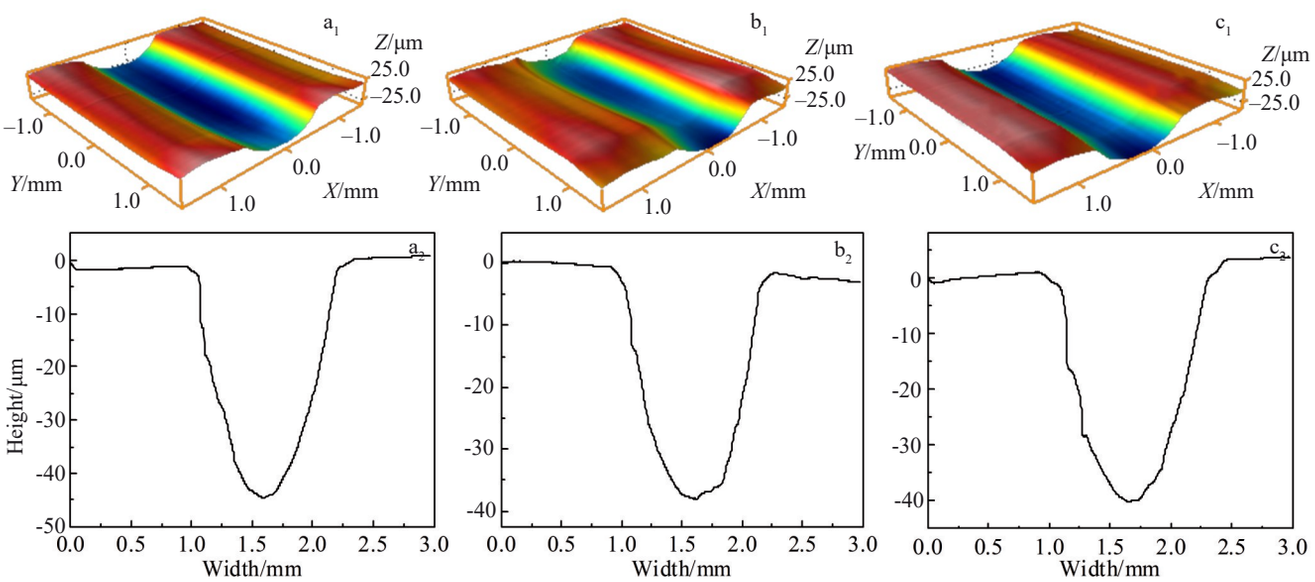

Fig.12 3D (a_1–c_1) and 2D (a_2–c_2) profiles of the wear scars of WC-10Co cemented carbides with different Ce contents after the reciprocating friction test: (a_1–a_2) 0wt%, (b_1–b_2) 0.5wt%, and (c_1–c_2) 1wt%

Table 4 Wear-related parameters of WC-10Co cemented carbides with different Ce contents

Ce content/ wt%	Depth/ μm	Width/ mm	Cross sectional area/$\times10^{-2}$ mm^2	Volume loss/mm^3
0	44.001	1.371	3.50	0.1747
0.5	37.386	1.351	3.08	0.1536
1	39.027	1.379	3.32	0.1656

In certain regions, severe fragmentation of WC particles leads to material removal, resulting in the formation of cracks and pits, along with comparatively wide wear scars. After adding the Ce, the wear scar morphology becomes significantly smoother, and almost no cracks or pits appear. In contrast, the morphology is the best when Ce content is 0.5wt%, while the wear scars of the cemented carbide with Ce content of 1wt% begin to show a small number of pits, but the wear scar morphology is better than that of the cemented carbide without Ce. Based on the first-principles calculations, the

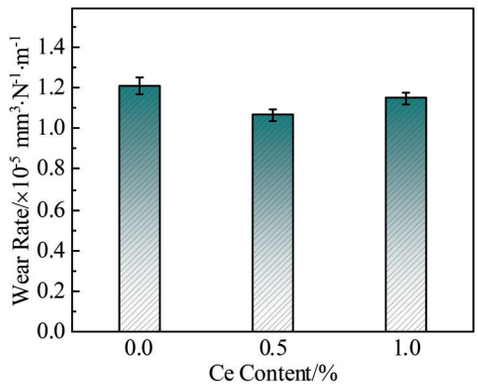

Fig. 13 Wear rates of WC-10Co cemented carbides with different Ce contents

interfacial bonding energy and interatomic bond strength of the WC/Co cemented carbide are inferior to those of the WC/CoCe cemented carbide, making its surface more susceptible to being worn away under the same friction conditions. Furthermore, key mechanical parameters of the parameters of WC/Co cemented carbide, including the bulk modulus to shear modulus ratio, Young ' s modulus, and Poisson ' s ratio, are all lower than those of the WC/CoCe cemented carbide. Therefore, its hardness, toughness, and plasticity are all inferior to those of the WC/CoCe cemented carbide, resulting in a lower relative density of the cemented carbide and the formation of pores. The increase in pores leads to the easy shedding of surface particles during friction, intensifying abrasive wear.

Fig. 15 shows SEM images and corresponding EDS

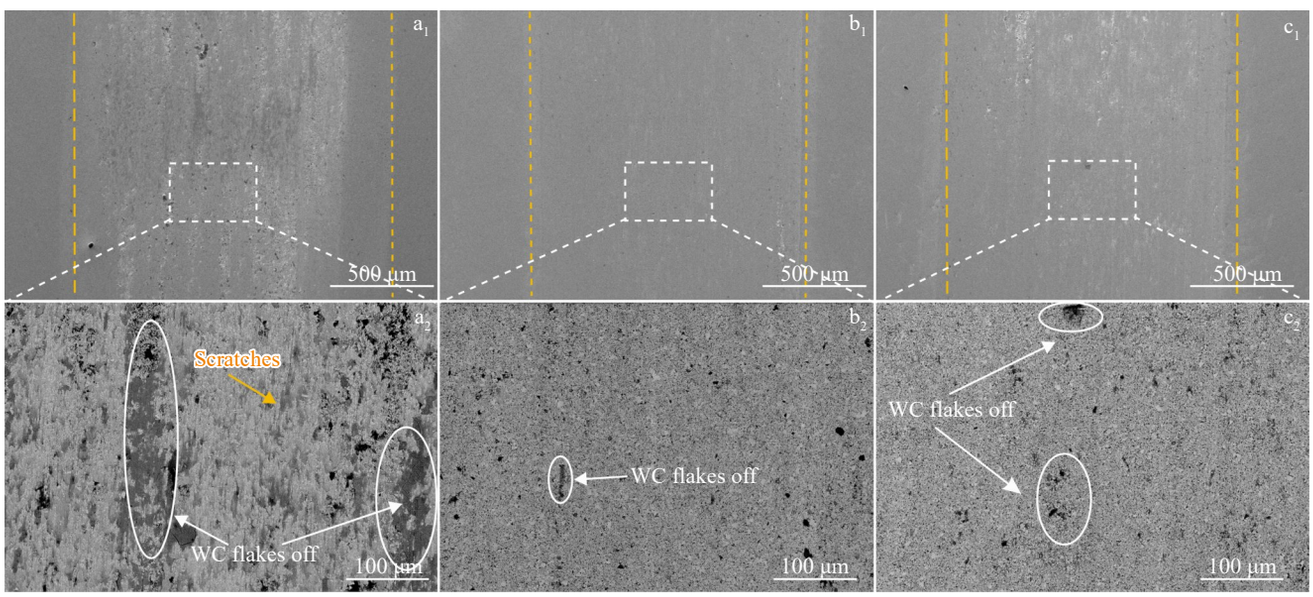

Fig. 14 SEM images of the wear scars of WC-10Co cemented carbides with different Ce contents after the reciprocating friction and wear test: (a_1–a_2) 0wt%, (b_1–b_2) 0.5wt%, and (c_1–c_2) 1wt%

elemental mappings of the wear scars in WC-10Co cemented carbides with different Ce contents. The elements W, C, Co, and Ce are uniformly distributed across the scanned area. In contrast, element O is predominantly concentrated within the wear scars of all the cemented carbides. The wear of the cemented carbides without Ce is the greatest, and the aggregation and distribution of element O at the wear scars are more obvious. The wear of the cemented carbide with 0.5wt% Ce is the least severe, and the content of element O at the wear scars is the least. The wear of the cemented carbides with 1wt% Ce is second-least severe. The element O begins to show several concentrated distribution phenomena at the abrasion scars. This oxygen enrichment can be attributed to high-temperature oxidation at the friction interface during testing. The WC-10Co cemented carbides without Ce possess a relatively low density, which results in poor intergranular cohesion and a tendency for grain pull-out, thereby accelerating wear. Furthermore, its comparatively lower hardness leads to deeper abrasion grooves and localized spalling, further exacerbating material loss. During the friction process, the scratches become deeper, and some parts flake off, which aggravates the wear of the cemented carbide. After adding an appropriate amount of element Ce, the comprehensive performance of the cemented carbide is uniformly improved, particularly in hardness and relative density. During the friction process, the grain cohesion is strong, so grains are not easily deformed and cracked. Therefore, compared with other samples, the cemented carbide with 0.5wt% Ce exhibits the lowest oxidation degree and superior wear resistance.

The addition of trace amounts of the rare-earth element Ce to WC-Co cemented carbides has been widely proven to be an effective method for significantly enhancing their overall performance. The underlying strengthening mechanism primarily stems from the synergistic effect of two core functions: grain refinement and interface purification. Firstly,

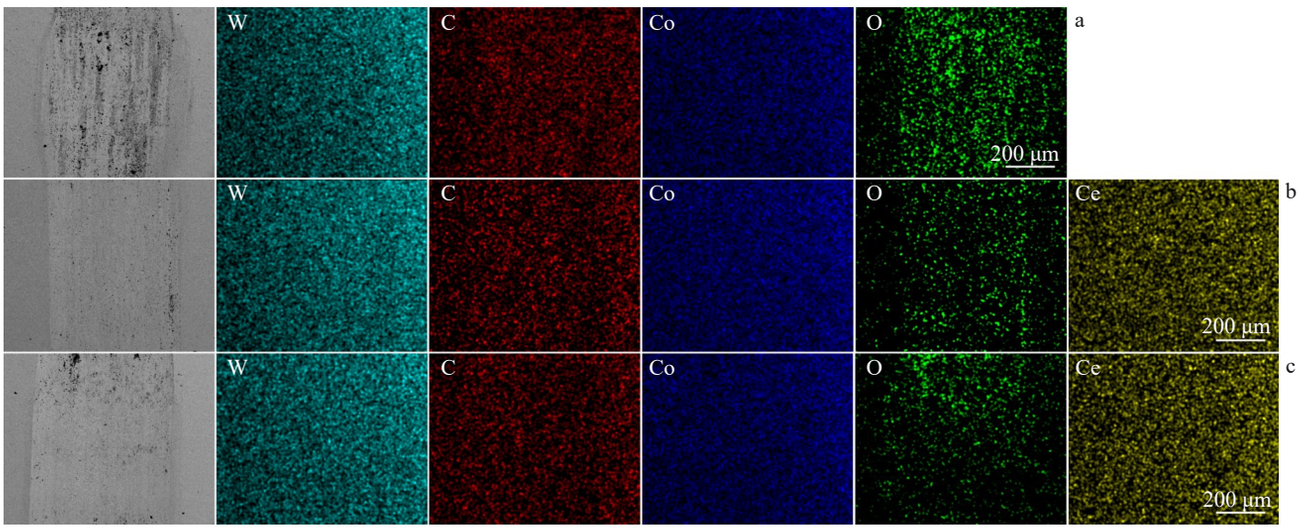

Fig. 15 SEM images and corresponding EDS element mappings of the wear scars of WC-10Co cemented carbides with different Ce contents: (a) 0wt%, (b) 0.5wt%, and (c) 1wt%

the element Ce directly strengthens the material matrix through grain refinement. As a surface active element, Ce preferentially segregates at the WC/Co phase boundaries during liquid-phase sintering. This segregation behavior effectively reduces the interfacial energy, thereby suppressing the Ostwald ripening process of WC grains via the dissolution-precipitation mechanism and fundamentally preventing abnormal grain coarsening. Simultaneously, trace amounts of Ce may form fine and uniformly dispersed rare earth compounds (such as Ce_2O_3, CeO_2, or complex carbides). These second-phase particles can effectively pin the grain boundaries, further inhibit grain-boundary migration, and ultimately result in a fine, uniform WC grain structure. Secondly, Ce significantly improves the toughness of material by refining the interfaces. Due to its extremely high chemical activity, Ce can react with impurity elements such as O and S introduced during raw material processing or sintering, forming stable, high-melting-point compounds[50] (e. g., Ce_2O_3 and CeS). This effectively removes these harmful impurities from the vulnerable grain and phase boundaries. The purified interfaces exhibit stronger bonding, significantly enhancing the hardness and fracture toughness of the material, as crack propagation requires more energy to break these robust interfaces[52].

When the Ce content is 0.5wt%, the optimal comprehensive performance is achieved through the synergistic effects of interface strengthening, grain refinement, and densification. Active Ce segregates at the WC/Co interfaces, purifies impurities, and forms strong covalent bonds, significantly enhancing interfacial bonding. Simultaneously, Ce or its oxide particles can pin grain boundaries and inhibit the growth of WC grains, which facilitates grain-refinement strengthening. Furthermore, a higher relative density (98.45%) is obtained during sintering, leading to concurrent improvements in hardness (1484 HV_{30}), toughness (10.55 $MPa \cdot m^{1/2}$), and wear resistance (wear rate of 1.067×10^{-5} $mm^3 \cdot N^{-1} \cdot m^{-1}$).

However, when the Ce content increases to 1wt%, Ce tends to agglomerate, forming coarse, brittle phases (such as Ce_2O_3). These phases not only hinder densification but also act as defects and crack initiation sites. As a result, the positive effects of grain refinement strengthening and interface strengthening are counteracted. Although its mechanical and wear properties remain superior to those of the Ce-free cemented carbide, they are slightly degraded relative to the optimal state with 0.5wt% Ce added.

In summary, the addition of 0.5wt% Ce, through the synergistic effects of grain refinement and interface purification, collectively promotes a comprehensive improvement in the mechanical properties and wear resistance of WC-Co cemented carbides.

5 Conclusions

1) Based on the calculated interfacial energy, elastic constants, and electronic properties of the cemented carbides before and after Ce addition, both structures exhibit mechanical stability. However, the WC-10Co cemented carbides with Ce addition demonstrate enhanced interfacial bonding, resulting in improved hardness and toughness, which effectively enhances the wear resistance of the material.

2) The bonding strength at the WC/Co and WC/CoCe interfaces is primarily contributed by atomic d-electron orbitals. According to the differences in DOS and local charge density, the proportion of covalent bonding increases after Ce addition, whereas metallic bonding dominates in the absence of Ce. Since covalent bonds possess higher bond energy than metallic bonds, structural stability is significantly improved with Ce incorporation.

3) The WC-10Co cemented carbide containing 0.5wt% Ce exhibits the most favorable microstructure, along with the highest hardness (1484 HV_{30}) and fracture toughness (10.55 $MPa \cdot m^{1/2}$), and a wear rate of 1.067×10^{-5} $mm^3 \cdot N^{-1} \cdot m^{-1}$. It demonstrates superior wear resistance under identical

testing conditions, which is consistent with the results obtained from first-principles calculations.

References

1 Prokopiv M M, Kharchenko O V, Uschapovskyi Y P *et al. Journal of Superhard Materials*[J], 2025, 47: 20

2 Tang Z X, Ge Z H, Li J. *Journal of Materials Science*[J], 2024, 59: 14621

3 Wachowicz J, Michalski A. *Composite Interfaces*[J], 2021, 28: 735

4 Ren X Y, Miao H Z, Peng Z J. *International Journal of Refractory Metals & Hard Materials*[J], 2013, 39: 61

5 Gren M A, Fransson E, Wahnström G. *International Journal of Refractory Metals & Hard Materials*[J], 2020, 87: 105114

6 Akkas M. *Materials Research Express*[J], 2020, 7: 076515

7 Xie Y J, Qi J J, Zhao M *et al. Journal of Alloys and Compounds*[J], 2025, 1021: 179640

8 Yang Y, Lu Z Y, Zan X *et al. International Journal of Refractory Metals & Hard Materials*[J], 2024, 119: 106545

9 Li Z L, Zhao W, Zhang D L *et al. Materials Research Express*[J], 2021, 8: 036512

10 Xia X Q, Gong M F. *Strength of Materials*[J], 2021, 53: 619

11 Li B, Li Y T, Guo Y *et al. Journal of Materials Engineering and Performance*[J], 2025, 34: 18634

12 Yang Y, Luo L M, Zan X *et al. International Journal of Refractory Metals & Hard Materials*[J], 2021, 98: 105536

13 Shu D, Cui X X, Li Z G *et al. Metals*[J], 2020, 10(2): 383

14 Lu Z Y, Qin Y Q, Zhu X Y *et al. International Journal of Refractory Metals & Hard Materials*[J], 2025, 131: 107209

15 Fu S, Xu Y X, Zhu L J *et al. Tribology International*[J], 2025, 205: 110524.

16 Yang Y, Lu Z Y, Zan X *et al. International Journal of Refractory Metals & Hard Materials*[J], 2023, 116: 106350

17 Liu J, Chen X K, Duan S J *et al. AIP Advances*[J], 2025, 15: 055127

18 Ge Y, Zheng C Y, Dai L J. *Journal of the Australian Ceramic Society*[J], 2024, 60: 525

19 Li H N, Zhang H M, Jiang Z Y. *Materials Today Communications*[J], 2024, 40: 109470

20 Fang Y, Wu M, Ci S N *et al. Physica B: Condensed Matter*[J], 2022, 646: 414336

21 Yang A C, Duan Y H, Peng M J *et al. Philosophical Magazine*[J], 2022, 102: 1

22 Wu Z X, Pang M J, Zhan Y Z *et al. Vacuum*[J], 2021, 191: 110367

23 Hao Z P, Qiu Y, Fan Y H *et al. International Journal of Refractory Metals & Hard Materials*[J], 2021, 101: 105688

24 Fan Y H, Li Z Y, Hao Z P. *Materials Science & Technology*[J], 2024, 41(13): 962

25 Hu T S, Yuan X M, Shi Z J *et al. Computational Materials Science*[J], 2020, 171: 109267

26 Yan Z B, Huang J B, Lei S Y *et al. Applied Surface Science*[J], 2025, 679: 161159

27 Zhang X Q, Yue Y L, Xu D *et al. Computational Materials Science*[J], 2023, 230: 112483

28 Li X, Qin X X, Lu S H *et al. International Journal of Refractory Metals & Hard Materials*[J], 2023, 111: 106075

29 Wu K J, Zhang Z Z, Liao H Y *et al. International Journal of Refractory Metals & Hard Materials*[J], 2023, 117: 106407

30 Zhang W G, Li Z L, Wei H *et al. Materials Today Communications*[J], 2022, 33: 104470

31 Eso O, Wang X, Wolf S *et al. International Journal of Refractory Metals & Hard Materials*[J], 2024, 118: 106482

32 Weidow J, Andrén H. *Acta Materialia*[J], 2010, 58: 3888

33 Weidow J, Andrén H. *International Journal of Refractory Metals & Hard Materials*[J], 2011, 29: 38

34 Ye Y W, Zhu B S, Zheng L Y *et al. International Journal of Refractory Metals & Hard Materials*[J], 2025, 129: 107099

35 Zhu B S, Zhang S F, Zheng L Y *et al. Ceramics International*[J], 2025, 51: 21621

36 Zavodinsky A V G. *International Journal of Refractory Metals & Hard Materials*[J], 2011, 29: 184

37 Fan Y H, Wang W H, Hao Z P. *Journal of Materials Engineering and Performance*[J], 2024, 33: 3582

38 Christensen M, Dudiy S, Wahnström G. *Physical Review B*[J], 2002, 65: 045408

39 Pandit A, Bongiorno A. *Computer Physics Communications*[J], 2023, 288: 108751

40 Zhang Z, Gao H Y, Zhang Z W *et al. Materials Today Communications*[J], 2024, 39: 109070

41 Wu Z J, Zhao E J, Xiang H P *et al. Physical Review B*[J], 2007, 76: 054115

42 Liu Y, Wang J, Gao Q N *et al. Journal of Central South University*[J], 2015, 22(5): 1585

43 Li M, Wang X, Liu K *et al. Advanced Energy Materials*[J], 2023, 13: 2301162

44 Bouhlala A, Doghmane M, Halais W T *et al. Modern Physics Letters B*[J], 2024, 38: 1

45 Li M F, Yu R K, Deng T Z *et al. Journal of Alloys and Compounds*[J], 2024, 1008: 176868

46 Huang Y T, Li X W, Zha Y F *et al. Materials Today Communications*[J], 2021, 28: 102550

47 Ignie C, Gee M G, Nunn J W *et al. Wear*[J], 2013, 302: 1050

48 Gee M, Mingard K, Nunn J *et al. International Journal of Refractory Metals & Hard Materials*[J], 2017, 62: 192

49 Tang Z Y, Cheng C, Chen L Y *et al. Tungsten*[J], 2025, 7(2): 314

50 He W, Tan D Q, Kuang H *et al. Journal of Alloys and Compounds*[J], 2018, 742: 702

51 Li M, Wei D, Hu H X *et al. Rare Metal Materials and Engineering*[J], 2025, 54(7): 1727

52 Deng C J, Lin F K, Yang T N *et al. Rare Metal Materials and Engineering*[J], 2025, 54(4): 886

WC-Co-Ce硬质合金的微观结构、力学和摩擦学性能：第一性原理计算和实验

李泽文[1,2]，陈　颢[1,3]，陈丽勇[1,3,4]，张建波[1]，张　帆[1]，谢小龙[1,3]

(1. 江西理工大学 材料科学与工程学院，江西 赣州 341000)

(2. 南昌工学院 教育学院，江西 南昌 330108)

(3. 江西理工大学 钨资源高效开发与应用技术教育部工程研究中心，江西 赣州 341000)

(4. 江西理工大学 稀有金属资源开发利用教育部与江西省协同创新中心，江西 赣州 341000)

摘　要：建立了WC/Co和WC/CoCe界面模型，利用第一性原理计算了界面能、弹性常数和电荷分布特征。采用液相烧结法制备了WC-10Co、WC-10Co-0.5Ce和WC-10Co-1Ce硬质合金。通过显微组织分析、力学性能测试和摩擦磨损测试，研究稀土元素Ce对硬质合金整体性能的影响。计算结果表明，Ce的掺杂促进了W和Ce原子在界面处形成强共价键，导致界面键能增加，界面能降低，结构稳定性提高。根据弹性常数和电子性能预测，合金的硬度、韧性和耐磨性都得到了提高。实验结果表明，当Ce含量为0.5wt%时，WC-10Co-0.5Ce硬质合金的性能最佳。在此浓度下，其维氏硬度达到1484 HV_{30}，断裂韧性为10.55 $MPa\cdot m^{1/2}$，磨损率为1.067×10^{-5} $mm^3\cdot N^{-1}\cdot m^{-1}$。

关键词：硬质合金；第一性原理；界面模型；力学性能；摩擦与磨损

作者简介：李泽文，男，1995年生，博士生，江西理工大学材料科学与工程学院，江西 赣州 341000，E-mail：1015811895@qq.com